# Extended Sacrificial Bulk Micromachining Process and Its Application to the Fabrication of X-axis Single-crystalline Silicon Micro-gyroscope

Jongpal Kim, Sangjun Park, Donghun Kwak, Hyoungho Ko, Taeyong Song , Dadi Setiadi*, William Carr*, James Buss**, and Dong-il Dan Cho

School of Electrical Engineering and Computer Science, Seoul National University,
San 56-1, Shinlim-dong, Kwanak-gu, Seoul 151-742, Korea
(Tel : +82-2-880-8371; E-mail: dicho@snu.ac.kr)
*New Jersey Microsystem, Inc., Newark, NJ, U.S.A.,
**Office of Naval Research, Arlington, VA, U.S.A.

**Abstract**: In this paper, we present a planar single-crystalline silicon x-axis micro-gyroscope fabricated with a perfectly aligned vertical actuation combs on one silicon wafer, using the extended SBM technology. The fabricated x-axis micro-gyroscope has the resolution of 0.1 deg/sec, the bandwidth of 100 Hz. These research results allow integrating 6 axes inertial measurement (3 accelerations and 3 angular rates) on the same silicon substrate using the same process for the first time.

**Keywords:** Extended Sacrificial Bulk Micromachining, x-axis gyroscope, vertical comb

## 1. INTRODUCTION

Planar x-axis MEMS gyroscopes have received much attention for multiple-axis sensing applications. The x-axis gyroscope detects the rotation rate about an axis parallel to the device substrate. This requires a combination of horizontal and vertical motion, which is very difficult to achieve in one single-crystal silicon wafer. A z-axis gyroscope requires only planar motions along x and y axes which is easily done. For example, we have reported several z-axis gyroscopes using the SBM process [1-3]. A planar y-axis gyroscope is easily obtained by rotating the x-axis gyroscope by 90 degrees in the mask layout. Then, a 3-axis gyroscope can be integrated on the same plane on a single wafer.

There have been 2 previous single-crystalline silicon x-axis gyroscopes using wafer bonding techniques [4, 5]. Both use lateral actuation using lateral combs, and vertical sensing using substrate bottom electrodes. In order to fabricate bottom electrodes, wafers must be bonded, and a complicated electrode connection scheme must be used. This paper uses high-aspect-ratio lateral electrodes for a high sensitivity, and vertical combs for vertical actuation. Since the SBM process can give a large (> tens of μm) sacrificial gap, the squeeze film damping does not become a problem. In addition, the SBM process completely eliminates footing, so structural degradation and electrical shorting from footing poses no problems. Note that there exist another processes for fabricating vertical combs, where upper and lower electrodes are fabricated on different wafers and bonded [6, 7]. Hence, misalignment can be a problem for high precision sensors.

This paper presents a planar, single-crystalline silicon x-axis gyroscope fabricated using only one wafer for the first time, using the extended Sacrificial Bulk Micromachining (SBM) technology. Our previously developed extended SBM process can fabricate vertically offset combs in single-crystalline silicon with no alignment error, by defining upper and lower combs in the same mask [8, 9]. This is very important for precision sensors. Previously reported vertical comb structure required at least two masks for defining upper and lower combs, which inevitably gives alignment errors. The fabricated x-axis gyroscope has a noise equivalent angle random walk of 0.01 deg/sec/$\sqrt{\text{Hz}}$ .

## 2. DESIGN OF X-AXIS SINGLE-CRYSTALLINE SILICON MICRO-GYROSCOPE

The x-axis micro-gyroscope fabricated using the extended SBM process, detects the input angular rate about an axis parallel to the device substrate. Figure 1(a) shows the schematic of the x-axis micro-gyroscope. The x-axis micro-gyroscope constitutes of vertical actuation comb, vertical actuation spring, outer mass, sensing spring, inner sensing mass, and lateral sensing comb. The outer and inner masses are actuated together in the z-direction at an actuation mode resonant frequency by the vertical actuation comb. When an angular rate is applied in the x-direction, the Coriolis force is generated in the y-direction. The movement of the outer mass in the y-direction is restricted because of high stiffness of vertical actuation spring in the y-direction. The only sensing mass can move in the y-direction by the Coriolis force. From the capacitance change induced by the sensing displacement, the angular rate can be estimated. The x-axis micro-gyroscope in Figure 1(a) is modeled as shown in Figure 1(b). The dynamic motion of the x-axis micro-gyroscope can be simplified as two degree of freedom system. When a z-axis actuation displacement of the x-axis micro-gyroscope is $z(t) = Z\sin\omega_a t$ and a x-axis angular rate input is $\omega(t) = \Omega\sin(\omega_\Omega t + \phi_\Omega)$, the y-axis displacement of the x-axis micro-gyroscope to the sensing direction is expressed as (1). In (1), $\omega_a$ is the resonant frequency of the actuation mode, $\omega_s$ is the resonant frequency of the sensing mode, $Q_s$ is the quality factor to the sensing mode.

$$
\begin{aligned}
y &= Y_+\sin\left[(\omega_a+\omega_\Omega)t+\phi_\Omega+\phi_+\right] \\
&\quad - Y_-\sin\left[(\omega_a-\omega_\Omega)t-\phi_\Omega-\phi_+\right] \\
Y_+ &= \frac{F_C}{\sqrt{\left((\omega_\Omega+\omega_a)^2-\omega_s^2\right)^2+(2\varsigma_s\omega_s)(\omega_\Omega+\omega_a)^2}} \\
Y_- &= \frac{F_C}{\sqrt{\left((\omega_\Omega-\omega_a)^2-\omega_s^2\right)^2+(2\varsigma_s\omega_s)(\omega_\Omega-\omega_a)^2}} \\
\tan\phi_+ &= \frac{\omega_s(\omega_\Omega+\omega_a)}{Q_s\left((\omega_\Omega+\omega_a)^2-\omega_s^2\right)} \\
\tan\phi_- &= \frac{\omega_s(\omega_\Omega-\omega_a)}{Q_s\left((\omega_\Omega-\omega_a)^2-\omega_s^2\right)} \\
F_c &= \Omega Z\omega_a
\end{aligned}
\qquad (1)
$$

Generally, a vertical motion structure is realized as a seesaw using a torsion beam. In this torsion system, when the one side of the structure moves up, the other side of the structure moves down. Only the rotational motion is applicable in the conventional torsion spring system. For using this rotational motion as the actuation mode, the sensing mode must also have the rotational motion in the x-axis micro-gyroscope. When the rotational mode is used for actuation and sensing, the problem of the rotational motion coupling between actuation and sensing modes must be solved. It is difficult to decouple this rotational motion between actuation and sensing modes in a comb-actuation and comb-sensing type. Recently, the vertically translational spring with a motion shape as shown in Figure 2(a) is proposed [10]. The thickness of this vertical spring becomes same with the structure thickness. However, the spring length is not required so long as the case of using the conventional straight beam spring. The vertical spring is placed at the x-axis and y-axis symmetrical position. This arrangement increases the x and y-axis translational stiffness and the x, y, and z-axis rotational stiffness. The end of the connection plate is attached at each center of two beams. When a center mass moves vertically, beams of the vertical spring are twisted and deflected. The beam of the vertical spring attached to the center mass can slide only to the z direction. The vertical stiffness is derived analytically with some approximations and compared with the simulated value. The actuation part of the x-axis micro-gyroscope is simply modeled as shown in Figure 2(b). The vertical spring is loaded by internal force and moment as shown in Figure 2(b). The deflection height can be expressed with the length SCH of connection plate between two spring beams and the twisting angle as (2). The internal moment Mt exerted to the vertical spring can be expressed with an external force FL and the length of connection plate SCH as (3). For the simple derivation of the vertical stiffness, the twisting motion of the spring beam is only considered except for the deflection of the spring beam. Also, we assume silicon as isotropic material for using of twisting angle equation (4) of isotropic material. From these assumptions and equations of (2), (3), and (4), the simple equation for the vertical stiffness can be expressed as (5), where k1 is a constant varying with the aspect ratio of the cross section of the spring beam, G is shear modulus, w is the width of the spring beam, t is the thickness of the spring beam, and la is the length of the spring beam.

$$\delta_z = SCH \cdot \phi \quad (2)$$

$$M_t = \frac{F_L \cdot SCH}{16} \quad (3)$$

$$\phi = \frac{M_t \cdot l_a}{k_1 \cdot G \cdot w^3 \cdot t} \quad (4)$$

$$k_z = \frac{16 \cdot k_1 \cdot G \cdot w^3 \cdot t}{l_a \cdot SCH^2} \quad (5)$$

The stiffness values using simple analytic equation is compared with the stiffness values using the ANSYS simulation in Figure 2(c). For the spring length la of 80, 120, and 160 ㎛, the z direction stiffness is simulated with respect to the length of the connection plate SCH of 200, 250, and 300 ㎛. For the spring length la of 80 and 120 ㎛, the stiffness derived from the analytic equation coincides well with the simulated stiffness. In the case of the spring length of 80 ㎛, the simulated stiffness is somewhat greater than the stiffness derived from the analytic equation. This mismatch causes from ignoring the deflection effect of the spring during the derivation of the analytic equation. As the spring length becomes longer, the vertical stiffness is governed dominantly by the torsion effect of the spring. As the spring length becomes shorter, the deflection effect of the spring increases the stiffness of the vertical spring.

The capacitance of the vertical comb is simulated with respect to the z-axis displacement for the investigation of linear characteristics. The simulation model is as shown in Figure 3(a). The nominal condition is as follows. The lateral gap between the upper and lower electrodes is 4 ㎛, vertical offset is 12 ㎛, thickness of structures is 30 ㎛, and overlap length is 400 ㎛. As 1 ㎛ increase of the z-axis displacement from – 18 ㎛ to + 12 ㎛, the capacitance of the vertical comb is plotted as shown in Figure 3(b). Using the capacitance data from – 5 ㎛ to + 5 ㎛, the least square fitted linear equation is derived. From comparing between this linear equation and simulated capacitances, the linear region ranges from – 11 ㎛ to 7 ㎛ within the nonlinearity of 1 %. This means that the vertical offset must be larger than the sum of the vertical displacement and the basic vertical offset of 5 ㎛ for below 1 % nonlinearity.

## 3. FABRICATION OF X-AXIS SINGLE-CRYSTALLINE SILICON MICRO-GYROSCOPE

The developed extended SBM technology is based on the SBM technology[11-13]. Therefore, the extended SBM technology includes all the characteristics of the SBM technology. Using the SBM technology, a (111) single-crystalline silicon high aspect ratio structure (HARS) can be fabricated with flat bottom surface and large sacrificial depth for lateral motion devices. Using the extended SBM process, a vertically offset (111) single-crystalline silicon HARS with different structure thickness can be fabricated for vertical motion devices. In the extended SBM process, although two photo masks are used, all the in-plane dimensions of structures are decided in the first photo mask. Therefore, there is no horizontal align error between the upper and lower electrodes. Through four steps of deep silicon etch, we can freely control the thickness of upper electrode and lower electrode, the vertical overlap or offset between the upper and lower electrodes, and the sacrificial depth. In addition, the extended SBM technology is processed with the conventional deposition and etch steps without the difficult steps such as wafer bonding, chemical mechanical polishing, and electroplating.

Process steps are shown in Figure 4. Processing uses a (111) silicon as a structure material. The first etch masking material, for example silicon dioxide or silicon nitride, is deposited and patterned. The thickness of the mask film should be as thin as possible to reduce stress effect in the silicon structure, and thick enough to resist the following process steps. To reduce residual stress of etch mask, the composite layer of silicon dioxide and silicon nitride can be used. All critical dimensions, including moveable electrodes, fixed electrodes, and planar gaps are defined in this step. The second etch mask, for example photoresist or silicon dioxide, is then patterned as shown in Figure 4(a). This second etch mask covers the patterns, which will serve as an upper structure. The second etch mask pattern is wider than the first by considering of the alignment error and minimum opening

area for normal silicon deep reactive ion etch (RIE). Typically, the second etch mask pattern of the upper structure is wider than the first by an amount of 1.5 ㎛, and the minimum lateral gap between vertically offset structures is gL = 4 ㎛. Note that minor alignment errors in this second lithography step do not affect the final lateral dimensions of the structure. The first etch mask is slightly etched to make a thickness difference in the first etch mask. During this first mask etch, the etch mask in the region of the upper structure is protected by the second etch mask, but the first etch mask in the region of the lower structure is etched. The thickness difference of the first etch mask must be greater than the required thickness in later processes, such as the over etch for removing the thin first etch mask on the lower structure and the fourth silicon RIE. Silicon is then etched to the desired depth d1 using deep RIE as shown in Figure 4(b). An additional thickness difference occurs in the first etch mask between the upper structure and the lower structure. This additional difference is determined by the selectivity and etching time of the silicon RIE. The second etch mask is stripped as shown in Figure 4(c). Performing the second deep silicon RIE by an amount of d2 define the thickness of the upper structures t1 as shown in Figure 4(d). The sidewalls are then passivated, by first depositing a passivation film, for example silicon oxide, silicon nitride, or composite of silicon oxide and silicon nitride, on the entire structure, and subsequently by anisotropically etching passivation films on the upward facing surfaces as shown in Figure 4(e). The substrate is further etched by deep silicon RIE by an amount d3 as shown in Figure 4(f), and sacrificial etch is then performed in an alkaline solution as shown in Figure 4(g). The amount etched in the third silicon RIE step d3, must be larger than that of the first silicon RIE step d1. The first etch masks facing upward are further etched until the top surface of the lower structure silicon is exposed as shown in Figure 4(h). However, the first etch mask on the upper structure remains, because the mask thickness of the upper structure is thicker than that of the lower structure as described earlier. The fourth deep silicon RIE step is performed by an amount d4 as shown in Figure 4(i). By controlling the depth of the fourth deep silicon RIE, the vertical overlap or the vertical offset between the upper and lower structures can be adjusted. Finally stripping the etch masks and sidewall passivation films gives electrode structures that are vertically offset as shown in Figure 4(j). The resulting dimensions are: thickness of upper structure t1 = d2, thickness of lower structure t2 = d1 + d2 – d4, vertical overlap between the upper and lower structures gv = d2 – d4, thickness of thicker structure t3 = d1 + d2, and vertical gap between substrate and lower structure = d3. For electrostatic actuation and sensing, electrodes need to be electrically isolated, and the triple-film isolation method [13], honey comb-shaped oxide post isolation method [14, 15], selective SOI implant method [16, 17], or SOI isolation method can be used. In this paper, the SOI isolation method is used for the electrical isolation of the x-axis micro-gyroscope.

Figure 5(a) shows SEM photographs of the fabricated x-axis micro-gyroscope on a (111) SOI wafer using the extended SBM process. Figure 5(b) shows the vertical spring. Figures. 5(c), (d), and (e) show the driving vertical combs to drive the mass vertically, close up view of the vertical combs, and the combs for sensing Coriolis motion, respectively. The fabricated x-axis micro-gyroscope dimensions are as follows. The thickness of the structure is 30 µm, sacrificial gap is 30 µm, thickness of the upper electrode is 30 µm, thickness of the lower electrode is 30 µm, vertical offset between the upper and lower electrodes is 12 µm, and lateral gap between the upper and lower electrodes is 4 µm.

## 4. MEASUREMENT RESULTS

The performance of the fabricated x-axis micro-gyroscope is experimentally evaluated using the measurement scheme as shown in Figure 6. The x-axis micro-gyroscope is modeled electrically as the capacitors in the dot-lined box. The detection circuit includes two charge amplifiers, two high pass filters, and differential amplifier. Each sensing electrode of the x-axis micro-gyroscope is electrically connected to the negative input of the charge amplifier. The proportional voltage to the capacitance in the sensing electrode is produced in the charge amplifier. The feedback capacitor has the capacitance of 0.5 pF. The output signal of the charge amplifier has DC and ac components. The DC component corresponds to the nominal capacitance of the sensing electrode and the parasitic capacitance between the sensing electrode path and the other electrical path. This DC component has no meaningful data for the angular rate input. The parasitic capacitance in the sensing electrode1 path is not equal to the parasitic capacitance in the sensing electrode2 path in the realized detection circuit. Because the gain and offset of two charge amplifiers is not identical, the outputs of the charge amplifiers with a same capacitance input have also somewhat different DC values. The direct input of these different DC levels from the charge amplifiers to the differential amplifier may make the output of the differential amplifier saturated. Therefore, this DC component is eliminated using the following high pass filter. On the other side, the ac component of the output from the charge amplifier has the angular rate information in the modulated form with the actuation resonant frequency. In our experimental measurement, the moving parts of the x-axis micro-gyroscope are connected to ground. Theoretically, if the moving parts have a zero resistance, there is no electrical signal in the moving parts. However, in reality, the resistance of the moving parts measured from one end of spring support to the other end is several tens of ohms. Therefore, an electrical signal with the same frequency and similar phase to the driving signal is induced in the moving parts. Moreover, the driving signal is induced to the charge amplifier negative input by the parasitic capacitance between the driving and sensing electrical paths. This common feedthrough noise can be reduced by the differential amplifier.

To enhance sensitivity, it is necessary to make the difference in the resonant frequencies of the sensing and actuation modes small. However, the decrease of the difference between the sensing and actuation resonant frequencies makes the bandwidth smaller and the phase delay larger. In this paper, for the stable operation of the x-axis micro-gyroscope, the frequency difference between the sensing and actuation resonant frequencies is tuned to about 30 Hz. To vibrate the gyroscope in the actuation mode of 5.72 kHz, a 0.4 volt peak-to-peak sinusoidal voltage with a 0.6 volt offset is applied to the vertical comb electrode. The sensing mode resonant frequency can be adjusted by changing the tuning voltage Vt. For Vt of 7.37 volts, the resonant frequency is measured to be 5.75 kHz, which is separated from the driving mode by approximately 30 Hz.

The fabricated x-axis micro-gyroscope is tested in a 60 mTorr vacuum chamber, which is installed on a rate table. The detection circuit shown in Figure 6 is implemented on a bread board. The output of the sensing circuit is connected to a spectrum analyzer. In the test, the sensing mode resonant frequency is tuned to be 30 Hz higher than the actuation mode.

Figure 7 shows the output of the spectrum analyzer when a 10 deg/sec, 30 Hz angular rate is applied to the x-axis micro-gyroscope. The peak with the largest amplitude is the actuation feedthrough signal, which appears due to overall effects of the parasitic capacitance between electrical paths and the non-identical performance of charge amplifiers. The second and third largest peaks correspond to the 30 Hz angular rate input. Note that the rate input signal is separate from the driving signal by 30 Hz. The first peak is eliminated by the synchronous demodulation circuit since this peak has a phase difference of about 90 degrees with output signal. In Figure 7, the amplitude of the angular rate input is more than 100 times larger than the noise floor, which gives the noise equivalent angular rate resolution of 0.1 deg/sec. The bandwidth is dependent on the frequency mismatch and the ambient vacuum level. The frequency response of the fabricated x-axis micro-gyroscope is shown in Figure 8. The bandwidth can be defined as the frequency, in which the response amplitude decrease as – 3 dB compared with the response amplitude in the DC input for the same angular rate input. The measured bandwidth is more than 100 Hz. The maximum response with respect to the angular rate input frequency appears at the frequency equal to the frequency difference value between the actuation and sensing modes. Therefore, the fabricated x-axis micro-gyroscope has a noise equivalent angle random walk of 0.01 deg/sec/$\sqrt{\text{Hz}}$ .

## 5. CONCLUSIONS

A single-crystalline x-axis micro-gyroscope with a vertical comb was fabricated on one (111) SOI wafer using the extended SBM technology for the first time. The extended SBM process described in this paper is possible to fabricate horizontally and vertically moveable single-crystalline structures for actuation and sensing using only one (111) Si. In the extended SBM process, although two photo masks are used, all the in-plane dimensions of structures are decided in the first photo mask. Therefore, there is no misalignment between the upper and lower electrodes. Through four steps of deep silicon etch, we can freely control the thickness of upper electrode and lower electrode, the vertical overlap between the upper and lower electrodes, and the sacrificial depth. In addition, the extended SBM technology is processed with the conventional deposition and etch steps without the steps such as wafer bonding and chemical mechanical polishing. The vertical spring having the same thickness with the structure thickness was characterized and designed for the vertical actuation. The array gap of unit capacitor in the sensing part was optimized for maximizing the sensing capacitance variation. A single-crystalline x-axis micro-gyroscope with a vertical comb was fabricated on one (111) SOI wafer. The thickness of the fabricated x-axis micro-gyroscope is 30 ㎛, the sacrificial gap is 30 ㎛, the thickness of the upper electrode is 30 ㎛, thickness of the lower electrode is 30 ㎛, vertical offset between the upper and lower electrodes is 12 ㎛, and lateral gap between the upper and lower electrodes is 4 ㎛. The performance of the fabricated x-axis micro-gyroscope is experimentally evaluated. The measured noise equivalent resolution was 0.1 deg/sec, and the measured bandwidth was 100 Hz. These research results allow integrating x, y, and z-axis gyroscopes on a singe wafer.


## ACKNOWLEDGMENTS

This research was supported by U.S. Navy under the contract number N00014-02-C-0126. This research was also supported by KOSEF Development of Telecmatics-based Integrated Sensing and Monitoring Systems Project.


## REFERENCES


[1] D. Cho, S. Lee, and S. Park, ”Surface/Bulk Micromachined High Performance Silicon Micro-gyroscope,” 2000 Solid-state Sensor and Actuator Workshop (Hilton Head), Late News, Hilton Head Island, SC, USA, June 2000.

[2] S. Lee, S. Park, J. Kim, S. Yi, and D. Cho, “Surface/Bulk Micromachined Single-crystalline Silicon Micro-gyroscope,” IEEE/ASME Journal of Microelectromechanical Systems, vol. 9, no. 4, pp. 557-567, Dec. 2000.

[3] J. Kim, S. Park, D. Kwak, H. Ko, W. Carr, J. Buss, and D. Cho, “Robust SOI Process without Footing for Ultra High-Performance Microgyroscopes,” Proceedings of Transducers 2003: 12th International Conference on Solid State Sensors and Actuators, pp. 1691-1694, Boston, USA, June 8-12, 2003.

[4] Y. Mochida, M. Tamura, and K. Ohwada, “A micromachined vibrating rate gyroscope with independent beams for the drive and detection modes,” Tech. Dig. Twelfth IEEE International Conference on Microelectromechanical Systems, Orlando, USA, January 17-21, 1999, pp. 618-623.

[5] B. Lee, S. Lee, K. Jung. J. Choi, T. Chung, and Y. Cho, “A de-coupled vibratory gyroscope using a mixed micro-machining technology, ” Proceedings of the 2001 IEEE International Conference on robotics & Automation, Seoul, Korea, May 21-26, 2001, pp.3412-3416.

[6] R. A. Conant, J. T. Nee, K. Y. Lau, and R. S. Muller, “A flat high-frequency scanning micromirror,” Tech. Dig. Solid-state Sensor and Actuator Workshop, Hilton Head Island, SC, USA, June 4-8, 2000, pp. 6-13.

[7] J. Lee, Y. Ko, H. Jeong, B. Choi, J. Kim, and D. Jeon, “SOI-based fabrication processes of the scanning mirror having vertical comb fingers, ” Sensors and Actuators A, Vol. 102, pp. 11-18, December 2002.

[8] J. Kim, S. Park, and D. Cho,., “A Novel Electrostatic Vertical Actuator Fabricated in One Homogeneous Silicon Wafer Using Extended SBM Technology”, Proceedings of Transducers 2001: 11th International Conference on Solid State Sensors and Actuators, pp. 756-759, Munich, Germany, June 2001.

[9] J. Kim, S. Park, and D. Cho, “A Novel Electrostatic Vertical Actuator Fabricated in One Homogeneous Silicon Wafer Using Extended SBM Technology”, Sensors and Actuators A, vol. 97-98, pp. 653-658, April 2002.

[10] S. Lee and J. Kim, “MEMS Gyroscope Having Mass Vibrating Vertically on Substrate”, Korean Patent Application No. 2001-0079496, 2001. 12. 4.

[11] S. Lee, S. Park, and D. Cho, “A New Micromachining Technology Using (111) Silicon,” Digest of Papers on Microprocess and Nanotechnology Conference, pp. 174-175, Kyungju, Korea, June 1998.

[12] S. Lee, S. Park, and D. Cho, “A New Micromachining Technique with (111) Silicon”, Japanese Journal of Applied Physics, vol. 38, pp. 2699-2703, May 1999.

[13] S. Lee, S. Park, and D. Cho, “The Surface/Bulk Micromachining (SBM) Process: A New Method for Fabricating Released Microelectromechanical Systems in Single Crystal Silicon”, IEEE/ASME Journal of Microelectromechanical Systems, vol. 8, no. 4, pp. 409-416, Dec. 1999.

[14] S. Lee, S. Park, and D. Cho, “Honeycomb-shaped Deep-trench Oxide Posts Combined with the SBM

Technology for Micromachining Single Crystal Silicon without Using SOI", Sensors and Actuators A, vol. 97-98, pp. 734-738, April 2002.
[15] S. Lee, S. Park, and D. Cho, "Honeycomb-shaped Deep-trench Oxide Posts Combined with the SBM Technology for Micromachining Single-crystal Silicon without Using SOI", Proceedings of Transducers 2001: 11th International Conference on Solid State Sensors and Actuators, pp. 1124-1127, Munich, Germany, June 2001.

[16] S. Park, S. Kim, J. Kim, S. Lee, S. Paik, C. Koo, and D. Cho, "A New Isolation Method for Single-crystalline Silicon MEMS Using Localized SOI Structure", Proceedings of the 3rd Korean MEMS Conference, pp. 129-135, Seoul, Apr. 2001.
[17] S. Park, J. Kim, D. Kwak, H. Ko, D. Cho, W. Carr, and J. Buss, "A New Isolation Method for Single Crystal Silicon MEMS and Its Application to z-axis Microgyroscope", Proc. International Electron Devices Meeting, Washington D.C., USA, Dec. 2003, accepted.

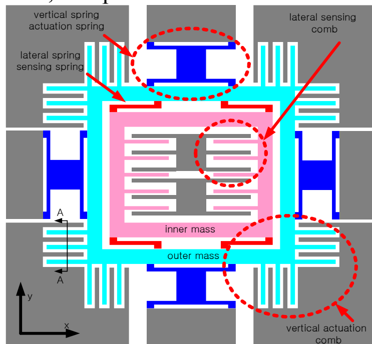


(a) Schematic of the x-axis micro-gyroscope

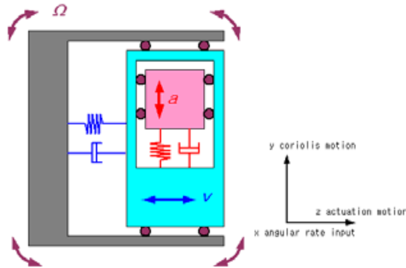


(b) Dynamic model of the x-axis micro-gyroscope

Figure 1. Schematic of the x-axis micro-gyroscope.

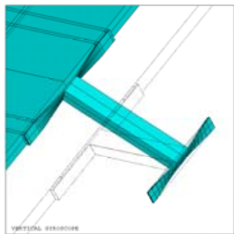

(a) Vertical motion of the vertical spring

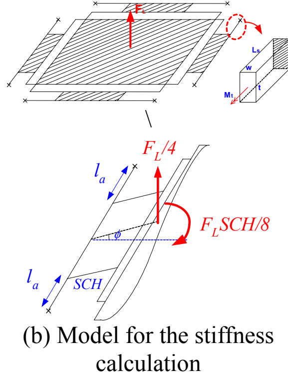


(b) Model for the stiffness calculation

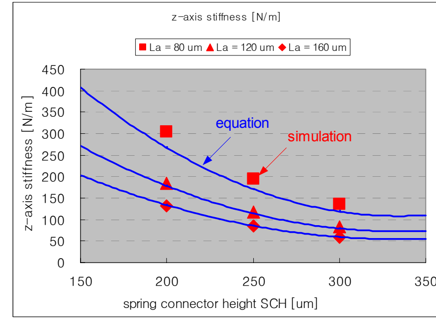


(c) Calculated and simulated vertical stiffness of the vertical spring

Figure 2. Vertical stiffness of the vertical spring.

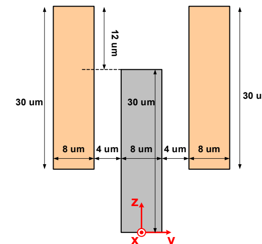


(a) The cross-section of the vertical comb

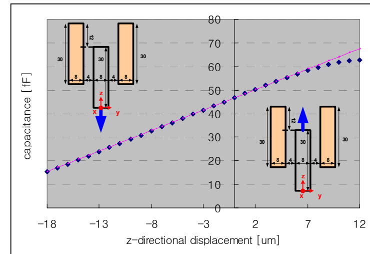


(b) Capacitance variation with respect to z-axis displacement

Figure 3. Linearity of the vertical comb

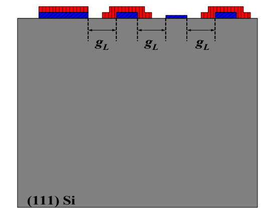


(a) first mask patterning and second mask patterning

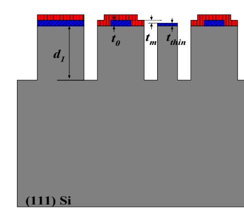


(b) first deep Si etch

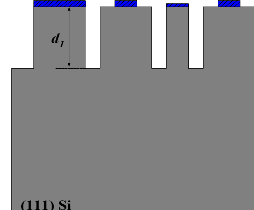


(c) second etch mask strip

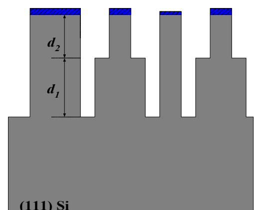


(d) second deep Si etch

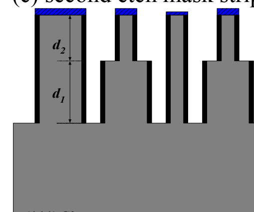


(e) sidewall passivation

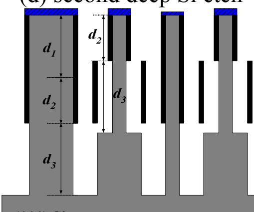


(f) third deep Si etch

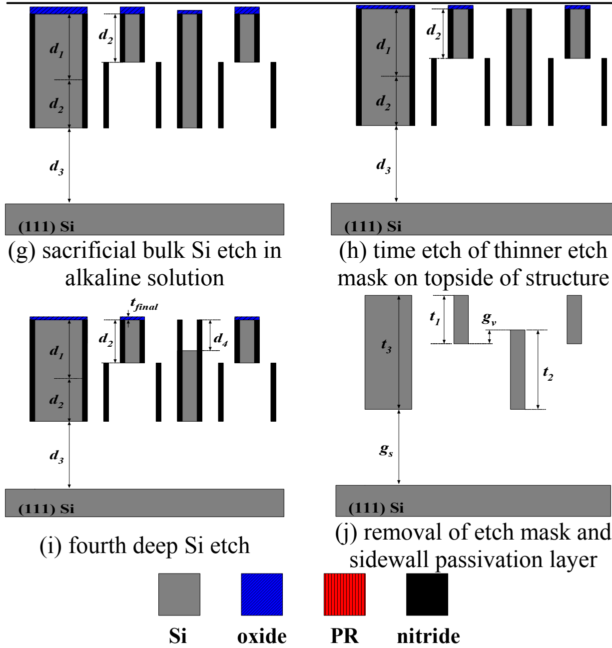


(g) sacrificial bulk Si etch in alkaline solution

(h) time etch of thinner etch mask on topside of structure

(i) fourth deep Si etch

(j) removal of etch mask and sidewall passivation layer

Figure 4. Process flow of the extended SBM process.

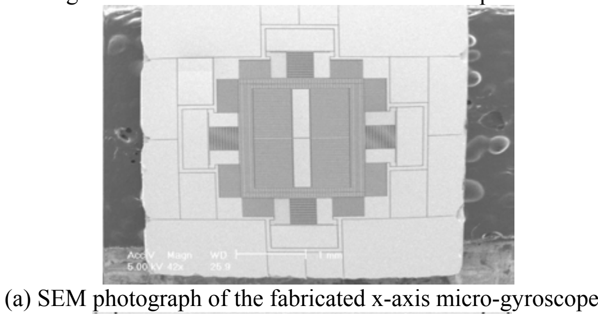

(a) SEM photograph of the fabricated x-axis micro-gyroscope

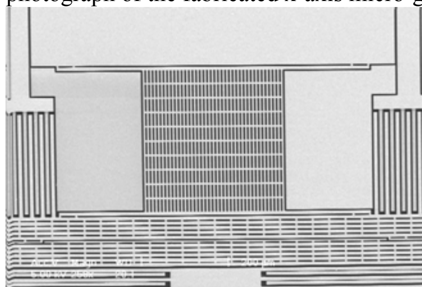

(b) close up view of the vertical spring

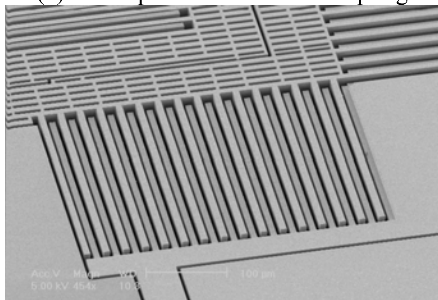

(c) close up view of the driving vertical combs

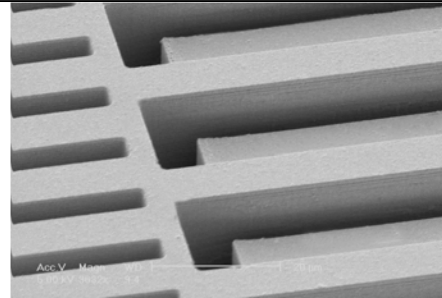

(d) close up view of vertical offset of the driving vertical combs

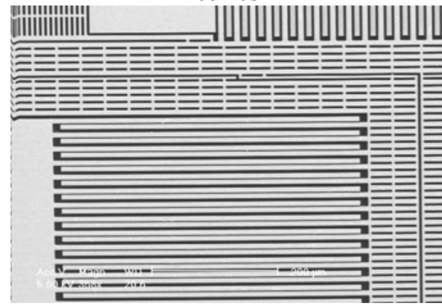

(e) close up view of combs for sensing the Coriolis motion

Figure 5. Fabricated x-axis micro-gyroscope using the extended SBM process.

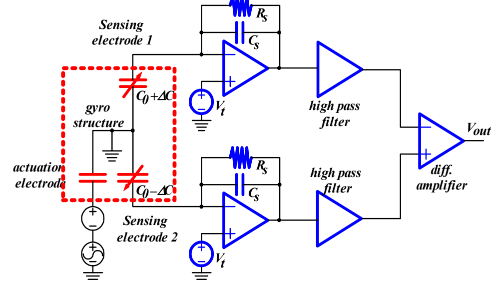


Figure 6. Detection circuit schematic for the performance test of the fabricated x-axis micro-gyroscope.

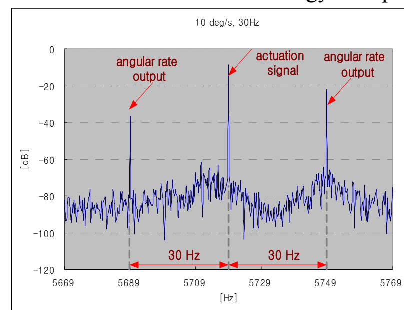


Figure 7. Frequency response of the fabricated x-axis.micro-gyroscope to 10 °/sec, 30 Hz angular rate input.

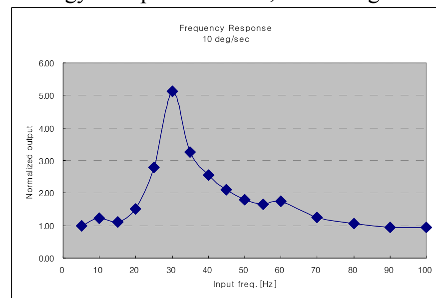


Figure 8. Response of the fabricated x-axis micro-gyroscope